Raman and fluorescence contributions to the resonant inelastic soft x-ray scattering on $LaAlO_3/SrTiO_3$ heterostructures

F. Pfaff,[1] H. Fujiwara,[2] G. Berner,[1] A. Yamasaki,[3] H. Niwa,[4] H. Kiuchi,[5] A. Gloskovskii,[6] W. Drube,[6] J. Gabel,[1] O. Kirilmaz,[1] A. Sekiyama,[2] J. Miyawaki,[4,7] Y. Harada,[4,7] S. Suga,[8] M. Sing,[1] and R. Claessen[1]

[1]*Physikalisches Institut and Röntgen Center for Complex Material Systems (RCCM), Universität Würzburg, D-97074 Würzburg, Germany*
[2]*Division of Materials Physics, Graduate School of Engineering Science, Osaka University, Osaka 560-8531, Japan*
[3]*Faculty of Science and Engineering, Konan University, Kobe 658-8501, Japan*
[4]*Institute for Solid State Physics, The University of Tokyo, Chiba 277-8581, Japan*
[5]*Department of Applied Chemistry, The University of Tokyo, Hongo, Bunkyo, Tokyo 113-8656, Japan*
[6]*DESY Photon Science, Deutsches Elektronen-Synchrotron, D-22603 Hamburg, Germany*
[7]*Synchrotron Radiation Research Organization, The University of Tokyo, 7-3-1 Hongo, Bunkyo-ku, Tokyo 113-8656, Japan*
[8]*Institute of Scientific & Industrial Research, Osaka University, Ibaraki, Osaka 567-0047, Japan*

(Received 5 September 2017; revised manuscript received 22 December 2017; published 8 January 2018)

We present a detailed study of the Ti 3*d* carriers at the interface of $LaAlO_3/SrTiO_3$ heterostructures by high-resolution resonant inelastic soft x-ray scattering (RIXS), with special focus on the roles of overlayer thickness and oxygen vacancies. Our measurements show the existence of interfacial Ti 3*d* electrons already *below* the critical thickness for conductivity. The (total) interface charge carrier density increases up to a $LaAlO_3$ overlayer thickness of 6 unit cells before it levels out. Furthermore, we observe strong Ti 3*d* charge carrier doping by oxygen vacancies. The RIXS data combined with photoelectron spectroscopy and transport measurements indicate the simultaneous presence of localized and itinerant charge carriers. At variance with previous interpretations, we show that in our excitation energy dependent RIXS measurements the amounts of localized and itinerant Ti 3*d* electrons in the ground state do not scale with the intensities of the Raman and fluorescence peaks, respectively. Rather, we attribute the observation of either Raman components or fluorescence signal to the specific nature of the *intermediate* state reached in the RIXS excitation process.

DOI: 10.1103/PhysRevB.97.035110

I. INTRODUCTION

Complex transition metal oxides exhibit a broad spectrum of intrinsic functionalities such as high-temperature superconductivity, colossal magnetoresistance, ferroelectricity, etc. Artificial layered structures made from such materials may even host novel phases not existing in the individual constituents. A prominent example is the formation of a high-mobility two-dimensional electron system (2DES) at the interface between a polar $LaAlO_3$ (LAO) film and a TiO_2-terminated nonpolar $SrTiO_3$ (STO) substrate, if the LAO thickness exceeds three unit cells (uc) [1,2]. The 2DES is formed by Ti 3*d* electrons, i.e., on the STO side of the interface [3], and a number of fascinating properties are reported: the 2DES can be controlled by electric field gating [4], becomes superconducting below 300 mK [5], and—most strikingly—can simultaneously display ferromagnetism [6,7], most likely related to the local moments of 3*d* electrons trapped by oxygen vacancies next to Ti sites [8,9].

While the exact mechanism for the 2DES formation is still under debate, there seems to be a wide consensus that the polar discontinuity at the LAO/STO interface plays a central role. A commonly discussed scenario is electronic reconstruction [10], viz. the redistribution of charge from the surface to the interface at and beyond the critical film thickness in order to compensate the electrostatic potential built-up across the LAO. Thus induced extra electrons are confined to the interface, populating the otherwise empty Ti 3*d* states. However, cation defects [11] and oxygen vacancies [12,13] have also been suggested as possible origins of the 2DES. Oxygen vacancies are known to act as electron donors in STO [14], and oxygen vacancy induced conductivity extending deeply into the substrate has indeed been observed for samples grown under low oxygen pressures [15]. Nonetheless, for heterostructures grown under higher oxygen pressures and/or post-oxidized samples, the conductivity remains finite but is confined to the interface region [3,16]. Despite many extensive studies, several crucial issues have remained unsolved. For instance, there are still questions concerning the charge carrier dichotomy possibly responsible for the coexistence of superconductivity and ferromagnetism and the electronic structure of samples with LAO films below the critical thickness.

Such heterointerfacial materials pose an exciting technical and methodological challenge to x-ray and electron spectroscopies since their use is only feasible if a specific interfacial contrast and a large enough probing depth can be accomplished at the same time. So far, photoelectron spectroscopy in the soft and hard x-ray regime has been successfully applied to various oxide heterostructures [3,17–19]. However, the need of sufficiently conductive samples to avoid charging and the limited probing depth preventing measurements on samples with overlayer thicknesses exceeding just a few nanometers are major disadvantages of the photoemission technique. Resonant inelastic x-ray scattering (RIXS) is appropriate to overcome these problems. As a photon-in/photon-out method,

it is bulk-sensitive and does not require intense efforts to prepare properly clean sample surfaces. In addition, it allows the measurement of highly insulating samples.

Previous studies have established that RIXS at the Ti L ($2p$) edge can provide valuable information on the relative amount of interfacial Ti $3d$ electrons in LAO/STO heterostructures [20,21]. By calibration against data from hard x-ray photoelectron spectroscopy (HAXPES), the sheet carrier densities derived from RIXS were found to be significantly higher than those obtained by Hall effect measurements [20]. This observation has been attributed to the coexistence of itinerant and localized Ti $3d$ electrons, which both give rise to the spectroscopic signals in RIXS and HAXPES while only mobile carriers are captured by the Hall coefficient [20]. In their RIXS study of LAO/STO superlattices, Zhou *et al.* even went a step further and argued that the Raman and fluorescence signals, which can be discriminated upon changing the excitation energy, can be used to distinguish between localized and itinerant Ti $3d$ carriers in the *ground state* [21].

In this paper, we present the results of a detailed high-resolution RIXS study of high quality LAO/STO heterostructures, probed with systematically varying photon energies. In agreement with the earlier superlattice results [21], we observe two prominent RIXS peaks involving the interfacial Ti $3d$ electrons, a localized dd excitation at a constant energy loss of around 2.3 eV (Raman signal) and a fluorescence component being almost independent of excitation energy. To further elucidate the origin of these two RIXS features, we analyze their behavior as a function of film thickness and oxygen stoichiometry and relate the results to complementary HAXPES and Hall effect data. Importantly, we find that the ratio of Raman and fluorescence contributions reflects the different degree of localization of the *intermediate* state—generally speaking being a superposition of quantum states of many different sites—in the RIXS process but not that of the initial state. We are thus led to conclude that RIXS cannot directly distinguish localized from itinerant Ti $3d$ carriers in STO-based heterostructures in the ground state, at variance with earlier suggestions [21].

II. EXPERIMENT

A series of LAO/STO heterostructures with LAO overlayer thicknesses from 2 to 20 uc were grown by pulsed laser deposition (PLD) on TiO_2-terminated STO(001) substrates. Laser ablation of a single crystalline LAO target was accomplished with a KrF excimer laser at a fluency of 1.1 J/cm^2 and a target-substrate distance of 56 mm. During the film growth the STO substrate was heated up to 780 °C, and the oxygen partial pressure was set to 1×10^{-3} mbar. In order to suppress unwanted oxygen vacancies the samples were treated by a post-oxidation (PO) procedure immediately after the growth (cooling stepwise down over a period of 2 hours from growth temperature to 360 °C in high oxygen pressure of 500 mbar). Besides, samples with a film thickness of 6 uc and various degrees of oxygen deficiency were grown by skipping the post-growth oxidation step (medium pressure growth = MP) and—to achieve even higher oxygen vacancy concentrations—by additionally reducing the oxygen partial pressure during growth to 5×10^{-7} mbar (low pressure growth = LP). Reference measurements were performed on commercially available bare STO crystals. All samples were characterized by standard *in and ex situ* methods including reflection high-energy electron diffraction (RHEED), atomic force microscopy (AFM), scanning transmission electron microscopy (STEM), temperature-dependent conductivity measurements, and x-ray photoelectron spectroscopy (XPS) as described elsewhere [22]. Based on this characterization, they are of the same high quality and behave as known from literature [15,22].

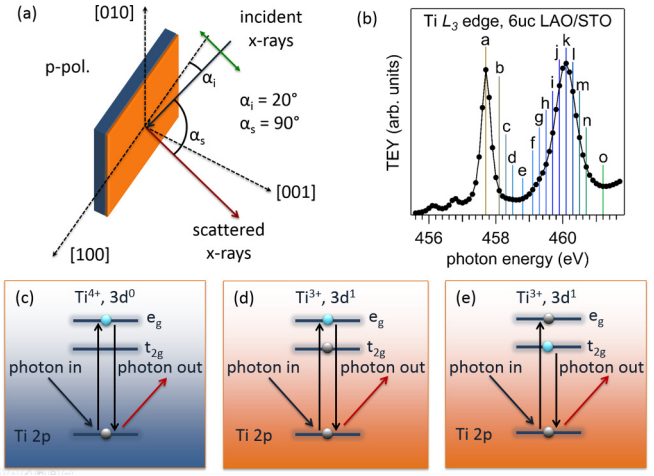

FIG. 1. (a) Sketch of the experimental geometry for XAS and RIXS measurements. Samples were aligned with the sample normal ([001] axis) lying in the scattering plane. The incident angle of the photons was set to 20° from the sample surface while the scattering angle was kept at 90°. The polarization vector of the incoming light was within the scattering plane (p polarization). (b) X-ray absorption spectrum at the Ti L_3 (Ti $2p_{3/2}$) edge of a 6-uc LAO/STO heterostructure measured in total electron yield mode. The used photon energies for RIXS measurements are marked by labels a-o. (c)–(e) Basic RIXS processes using photons tuned to, e.g., the e_g resonance. The electron depicted in blue is involved in the deexcitation process. (c) Only elastic scattering occurs for Ti ions in a $3d^0$ configuration (Ti^{4+}). (d, e) Beside elastic scattering (d) also inelastic scattering (e) is possible for Ti ions in a $3d^1$ configuration (Ti^{3+}), ending in an excited state with an electron in the e_g-manifold and observable as energy loss peak in the RIXS spectra.

The RIXS and x-ray absorption (XAS) measurements were performed at BL07LSU of SPring-8. A detailed description of the experimental setup can be found in Ref. [23]. All measurements were carried out at room temperature. The experimental geometry for both, RIXS and XAS, is depicted in Fig. 1(a). The angle of x-ray incidence was set to 20° with respect to the sample surface while the scattering angle was kept at 90° with respect to the incoming beam. The polarization vector was chosen to lie within the scattering plane (p polarization). By fitting the elastic line of bare STO with a Gaussian the energy resolution was determined to be ≈90 meV. The probing depth with the chosen geometry amounts to about 20 nm [20]. In order to reduce photon-induced oxygen depletion [24], the photon spot with vertical and horizontal dimensions of ∼2 μm × 90 μm was moved in vertical direction across the

sample surface by 10 μm every 30 minutes. No significant changes were observed in the spectra within this timescale.

An XAS spectrum at the Ti L_3 edge of a PO sample with an overlayer thickness of 6 uc measured in total electron yield mode is shown in Fig. 1(b). The photon energies selected for the RIXS measurements are marked by labels *a* to *o*. The two peaks centered at energies *a* and *k* reflect the cubic crystal-field splitting of the Ti 3*d* states of the STO substrate and are assigned to transitions from the Ti 2*p* core level into the $3d_{t_{2g}}$ and $3d_{e_g}$ states, respectively.

RIXS is a two-step process involving a photoexcitation of a core electron into unoccupied conduction band states and a subsequent decay of the excited state by emitting an x-ray photon. At the Ti *L* edge, after the excitation of an electron from the Ti 2*p* to the Ti 3*d* shell, different radiative decay channels are possible resulting in final states with different electronic configurations. The emitted photon can be elastically scattered with the final state being the original ground state [Figs. 1(c) and 1(d)]. Alternatively, an inelastic signal is observed when the system remains in an excited final state with, e.g., one electron in an e_g state and no electron in the t_{2g} manifold as depicted in Fig. 1(e). However, the latter process can only occur, if there is already one *d* electron in the initial state. Consequently, such a Raman signal is a measure of the finite 3*d* electron occupation as has already been shown for other titanates [25,26] and also for LAO/STO heterostructures [20] and superlattices [21].

Complementary photoemission experiments have been performed at the HAXPES endstation of beamline P09 at PETRA III (DESY, Hamburg), equipped with a SPECS Phoibos 225HV spectrometer. At the used photon energy of 3.5 keV, an overall energy resolution of 450 meV and a probing depth of about 12 nm—which is calculated as three times the inelastic mean free path according to Ref. [27] and by taking in addition the escape angle off normal emission into account—was realized. A detailed description of the beamline can be found in Ref. [28].

III. RESULTS

A. Excitation energy dependence

Two series of RIXS spectra of a bare STO substrate and a post-oxidized LAO/STO heterostructure with a 6-uc-thick film, recorded at photon energies across the Ti *L* edge and normalized to acquisition time, are displayed in Figs. 2(a) and 2(b), respectively. The labels *a*-*o* correspond to the excitation photon energies marked in the absorption spectrum of Fig. 1(b). In the language of a simple TiO_6 cluster model approach [29,30], the final state for the bare STO sample after the decay following the initial photoabsorption can be either $2p^63d^0$ or $2p^63d^1\underline{L}$ with $\underline{L}$ denoting a hole in the ligand O 2*p* shell. Beside the elastic line and the onset of the $3d^1\underline{L}$ charge transfer excitations at an energy loss of ≈3.5 eV [the full energy range from 3.5 to 18.0 eV energy loss is depicted in Figs. 3(a) and 4(a) for two different photon energies], no additional signal can be discerned throughout the photon energy series as shown in Fig. 2(a). In LAO/STO samples with films above the critical thickness, the ground state is partially of the type $2p^63d^1_{t_{2g}}$ due to the extra electrons in the 3*d* shell at the conducting interface.

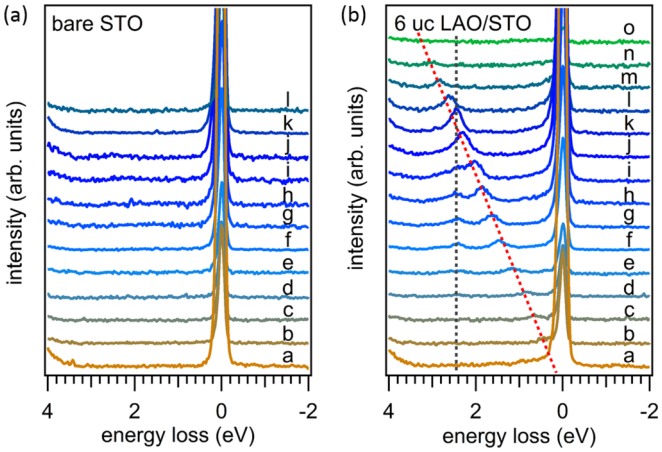

FIG. 2. Series of RIXS spectra. The labels *a*-*l* and *a*-*o* in (a) and (b) correspond to the excitation energies marked in the XAS spectrum in Fig. 1(b). (a) Series of RIXS spectra of a bare STO sample excited across the Ti *L* edge. The spectra are normalized by acquisition time. (b) Series of RIXS spectra of a 6-uc LAO/STO heterostructure excited across the Ti *L* edge. The spectra are normalized by acquisition time. The black and the orange dashed lines are guides to the eye marking the energies of the Raman and the fluorescence spectral features, respectively.

This results in an additional contribution to the RIXS spectra depending on the used excitation energy. In the case of the t_{2g} resonance (label *a*), the excited intermediate state will have the configuration $2p^53d^2_{t_{2g}}$. Two different final states are possible either contributing to the elastic line ($2p^63d^1_{t_{2g}}$) or to the charge transfer excitations with an energy loss above 3.5 eV represented by $2p^63d^2_{t_{2g}}\underline{L}$.

By increasing the incoming photon energy to the e_g resonance (label *k*), $2p^5t^1_{2g}e^1_g$ intermediate states can result via an additional decay channel in excited final states of the type $2p^63d^1_{e_g}$ [see Fig. 1(e)]. Thus inelastic intensity due to intraatomic *dd*-excitations from t_{2g} to e_g states becomes visible at an energy loss of around 2.3 eV, providing spectroscopic sensitivity to the interfacial Ti 3*d* carriers [Fig. 2(b)]. When changing the excitation energy from the t_{2g} towards the e_g resonance, we can actually identify two different signals, overlapping near the e_g resonance. While one signal shows a constant Raman shift of approximately 2.3 eV, the second signal exhibits fluorescence-like behavior resulting in a linear shift with incident photon energy in the energy loss plot of Fig. 2(b). Similar results have already been obtained by performing excitation energy dependent RIXS on LAO/STO superlattices [21] and other oxides like $BaTiO_3$ and $BaSO_4$ [31] or on $La_xSr_{1-x}TiO_3$ [26]. In the case of the superlattices, the authors attributed the observation of a Raman signal to localized charge carriers in the initial state, whereas the fluorescence signal was assigned to delocalized electrons in the system [21]. At variance with this interpretation, the authors of Ref. [31] assign the observation of Raman scattering in $BaTiO_3$ and $BaSO_4$ to a process where the excited electron is promoted to an unoccupied state and remains localized at the same atomic site on the timescale of the deexcitation, while the appearance of a fluorescence signal is ascribed to the delocalized character of the state reached by the excited

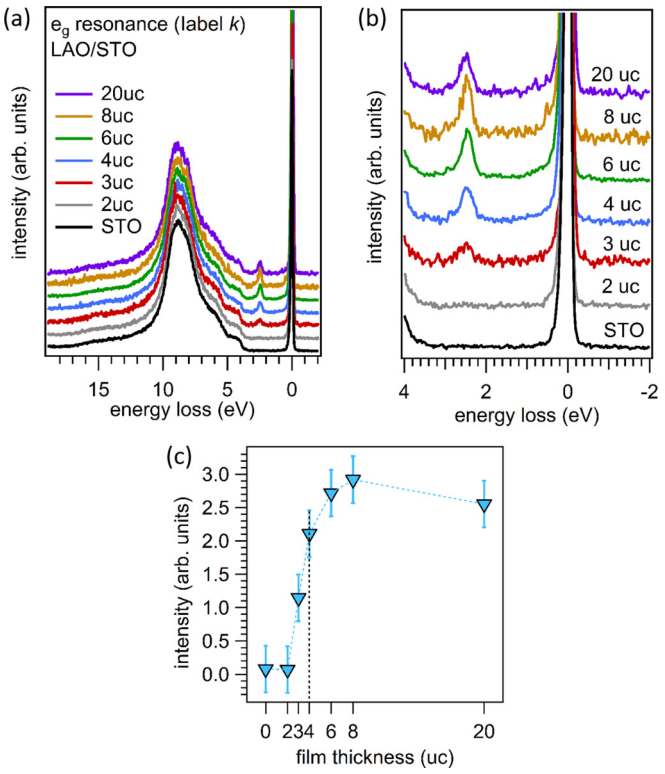

FIG. 3. (a) RIXS spectra measured at the e_g resonance of a bare STO sample and LAO/STO heterostructures with various overlayer thicknesses. The spectra are normalized to the $3d^1\underline{L}$ charge transfer excitations. (b) Low-energy region of the RIXS spectra in Fig. 3(a). (c) Spectral weight of the structure around 2.3 eV in Figs. 3(a) and 3(b) from a fitting analysis plotted against the film thickness.

electron in the intermediate state. We note that in this scenario either signal is proportional to the amount of 3*d* electrons. Thus further detailed experiments are required to clarify the origin of the features seen in the RIXS spectra of LAO/STO.

B. Thickness dependence

To further elucidate the nature of the two RIXS features, we performed detailed measurements at the e_g resonance on post-oxidized (PO) samples with overlayer thicknesses between 2 and 20 uc as well as on bare STO as a reference. The results are displayed in Figs. 3(a) and 3(b) showing a strong LAO thickness dependence of the spectra in the low-energy region up to the onset of the charge transfer excitations at 3.5 eV. The charge transfer excitations originate mainly from deep in the STO substrate far away from the interface region, are therefore essentially constant for the whole set of samples and thus can be used for data normalization.

For a quantitative account, the RIXS signals at a loss energy of about 2.3 eV [see Fig. 3(b)] have been fitted by Gaussians and the obtained integral intensities are plotted as a function of overlayer thickness in Fig. 3(c). The lack of any inelastic intensity for bare STO and the subcritical 2-uc sample shows the absence of Ti ions with a $3d^1$ configuration, i.e., with an extra valence electron, in the initial state. Although the photon-induced generation of oxygen vacancies, i.e., extrinsic electron doping, is minimized by moving the sample stepwise during the measurements, spectral weight is clearly visible for the insulating 3-uc sample. Since we do not observe any RIXS signal for the insulating 2-uc sample we consider the observation of an inelastic signal for samples with LAO film thicknesses in the range between 3 and 20 uc intrinsic to the measured heterostructures. Discrepancies in this respect between the present and previous RIXS measurements [20], which do show finite inelastic spectral weight for the insulating 2-uc heterostructure, likely can be attributed to a small amount of oxygen vacancies in the samples investigated in the latter. These are caused by the intense synchrotron radiation and become observable if the same sample spot is constantly exposed to the beam as in the previous study [20].

The RIXS intensity for the insulating 3-uc sample in the present experiment [see Fig. 3(b)] rather has to be explained by the presence of *localized* electrons that are not due to oxygen vacancy doping. This is in line with photoemission measurements showing the appearance of Ti 3*d* carriers already below the critical thickness for metallic transport [32]. In support of this scenario, x-ray linear dichroism reveals an orbital reconstruction at the interface also for an insulating 2-uc sample which has been interpreted as being due to symmetry breaking at the interface and the transfer of localized electrons to interface states [33]. Our findings are also consistent with the critical thickness of 3 uc for ferromagnetism—probably due to the existence of local Ti 3*d* moments—observed by Kalisky *et al.* in overlayer thickness dependent scanning SQUID measurements [34].

The observed RIXS intensity increases continuously with LAO film thickness and saturates at a thickness of 6 uc. In contrast, the mobile charge carrier concentrations obtained from Hall measurements show a sharp *steplike* behavior at the critical thickness of 4 uc [2]. This discrepancy has been attributed in previous experimental and theoretical studies to photogenerated charge carriers and/or the simultaneous presence of delocalized and localized charge carriers where the latter are not observed in transport [3,20].

Since the inelastic signal at the e_g resonance is actually a superposition of two features as can be recognized from Fig. 2(b), we focus in the following on measurements using an excitation energy 1 eV below the e_g resonance (label *f*), where the Raman and fluorescence components are well separated. The spectra recorded under this condition are depicted in Figs. 4(a) and 4(b) for the full set of samples. As selectively shown for the 6-uc sample in Fig. 4(c), the spectrum in this region contains at least seven components including the contribution of the charge transfer excitations at energies above 3.5 eV (gray shaded). In addition to the elastic line at zero loss energy (orange shaded), the fluorescence component at 1.4 eV (green shaded) and the two highest *dd* excitations at 2.9 and 2.4 eV (purple shaded) can be distinguished owing to the high energy resolution. Two lower lying *dd*-excitations at 0.6 and 0.2 eV (purple shaded) can also be discerned which, however, are not well resolved and probably overlap partially with spectral weight from scattering due to phonons. The four excitations ascribed to *dd* excitations reflect the complete lifting of the Ti 3*d* degeneracy. By carefully fitting the data with Gaussian line shapes, the energies of the *dd* excitations on the Ti^{3+} ions are determined to be 0.2, 0.6, 2.4, and 2.9 eV with an accuracy of ±0.1 eV. In a one-particle picture, from

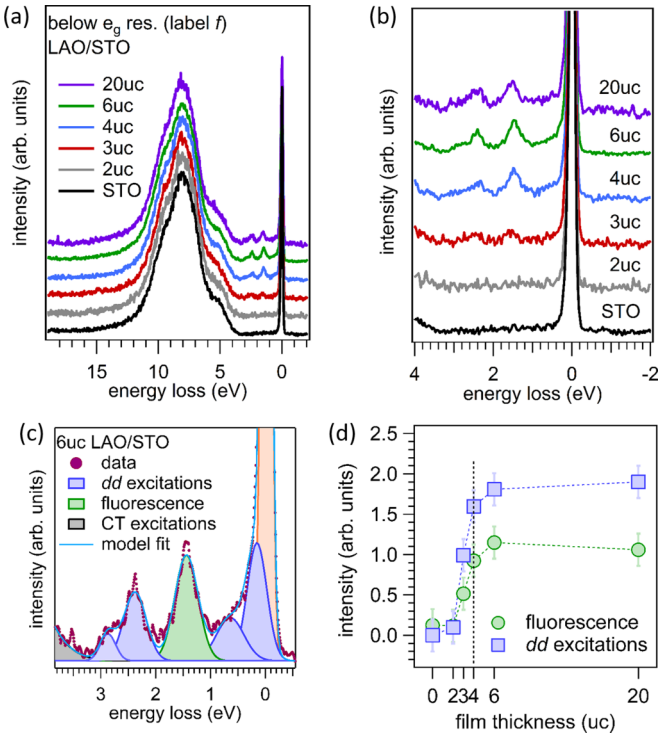

FIG. 4. (a) RIXS spectra of bare STO and LAO/STO heterostructures with varying LAO overlayer thickness measured 1 eV below the e_g resonance. The spectra are normalized to the $3d^1\underline{L}$ charge transfer excitations. (b) Low-energy loss region of the spectra in Fig. 4(a). (c) Fit analysis of the off-resonance RIXS spectrum of the 6 uc LAO/STO sample using seven Gaussian peaks. (d) Inelastic spectral weight of the *dd* excitations and the fluorescence feature obtained from the fitting of the RIXS spectra in Figs. 4(a) and 4(b), plotted as function of LAO overlayer thickness.

these values the energy of the lowest to the highest t_{2g} orbitals can be estimated to be (0.6 ± 0.1) eV and the e_g splitting as (0.5 ± 0.1) eV. These numbers significantly exceed those determined from x-ray absorption for the interface Ti^{4+} ions [35]. RIXS measurements of the *dd* excitation energies in LAO/STO superlattices, now again representative for the (distorted) $Ti^{3+}O_6$ octahedra at the interface, yield values for these energy splittings similar to ours [21]. The larger values, i.e., the larger crystal-field strength as compared to $Ti^{4+}O_6$ octahedra, were attributed in this study to an enhanced Coulomb repulsion and covalency between Ti $3d$ and O $2p$ states due to the extra occupation of the Ti $3d$ shell [21].

To establish quantitative correlations between the intensities of the inelastic signals, the spectra of the whole series of samples [see Fig. 4(b)] have been fitted taking seven Gaussian profiles into account as already explained above [cf. Fig. 4(c)]. As all four *dd*-excitations display the same dependence on LAO thickness within experimental accuracy their intensities have been summed up for clarity and better statistics. The total Raman intensity and the intensity of the fluorescence peak are plotted as a function of film thickness in Fig. 4(d).

Essentially, no RIXS intensity is discernible for bare STO and the 2-uc LAO/STO sample, pointing to the absence of $3d$ charge carriers within the accuracy of our experiment. The total RIXS spectral weight increases with larger overlayer thicknesses and saturates for a film thickness beyond 6 uc. Thereby, the intensity ratio of the fluorescence signal and the *dd* excitations stays virtually constant. The parallel rise in intensity of both signals up to 6 uc in contrast to the steplike increase of the mobile charge carrier concentration at 4 uc as observed in Hall measurements [2] compromises the attribution of either of the two observed features to *delocalized* and the respective other to trapped ground state electrons in LAO/STO heterostructures. Also the finite Raman *and* fluorescence spectral weights for the nonconducting 3-uc sample contradicts such an interpretation. Since both structures show basically the same dependence on film thickness they rather seem to reflect the total charge carrier concentration, including contributions by photogenerated charge carriers, as has been pointed out before for RIXS measurements on the e_g resonance where Raman and fluorescence peak overlap [20].

C. Influence of oxygen vacancies: electron doping

Since oxygen vacancies are known to act as electron donors we also studied 6 uc samples with an intentionally higher amount of oxygen vacancies to further clarify the origin and character of the two observed RIXS features. A higher oxygen vacancy concentration was accomplished as described in section II. In Fig. 5(a), the RIXS spectra—normalized to the $3d^1\underline{L}$ charge transfer excitations above 3.5 eV (not shown)—show a rise of both the Raman and fluorescence spectral weights with increasing oxygen vacancy concentration. As obtained from a fitting procedure equivalent to the one illustrated for the thickness dependent series of spectra in Fig. 4(c), the fluorescence component and the integrated spectral weight of all *dd* excitations rise *in the same proportion* with the amount of oxygen vacancies [see Fig. 5(b)]. Since both inelastic features are present in the spectrum for the fully oxidized sample (PO) with essentially only mobile electrons, neither component can be directly correlated with the amount of oxygen vacancies. However, the finite spectral weights of fluorescence and *dd* contributions for the PO sample can be readily considered as reflecting the intrinsic charge of the 2DES owing to electronic

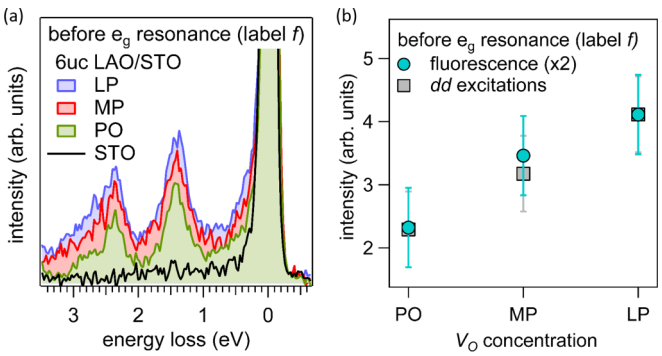

FIG. 5. (a) Series of RIXS spectra for samples with varying oxygen vacancy concentration normalized to the $3d^1\underline{L}$ emission. PO, MP, and LP refer to post-growth oxygen annealing, growth in medium and in low oxygen pressure (see Sec. II). (b) Intensities of the *dd* excitations and fluorescence signal (multiplied by a factor of 2) obtained by fitting of the RIXS spectra. Both increase in parallel with the oxygen vacancy concentration.

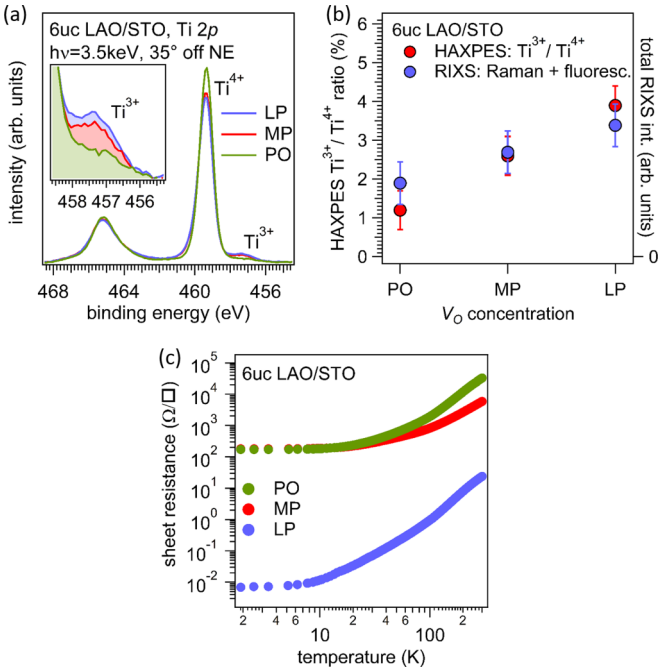

FIG. 6. (a) HAXPES Ti $2p$ spectra for the PO, MP, and LP samples recorded at an emission angle of 35° off normal emission. (b) Comparison of the Ti^{3+}/Ti^{4+} ratio obtained from fitting the Ti $2p$ spectra and the total RIXS intensity (sum of dd excitations and fluorescence feature). Note that there is no scaling associated with the abscissa except that the V_O concentration is increasing from the left to the right. (c) Temperature-dependent sheet resistance of the PO, MP, and LP samples.

reconstruction. If these offsets are subtracted, the increase of the intensities of dd excitations and fluorescence signal for the MP and LP samples apparently correlate with the additional electrons doped into the system by oxygen vacancies.

Figure 6(a) shows corresponding HAXPES Ti $2p$ core-level spectra normalized to the overall integrated intensity. Beside a strong Ti $2p_{3/2}$ peak due to emission from Ti^{4+} ions mainly in the STO bulk, a chemically shifted contribution from Ti^{3+} ions at the interface is visible at smaller binding energies. This signal is a measure for the extra electrons occupying the otherwise empty Ti $3d$ states and therefore reflects the total amount of charge carriers in the system [3]. By increasing the amount of oxygen vacancies, a strong increase in the total amount of charge carriers is observed in HAXPES as is better seen from the close-up of the Ti^{3+} weight in the inset of Fig. 6(a).

The Ti^{3+} weight normalized to the Ti^{4+} contribution as obtained from the fitting of the Ti $2p$ core-level HAXPES spectra of the three samples together with the total RIXS intensity (sum of the integrated weights of the dd excitations and the fluorescence component) are displayed in Fig. 6(b). After normalizing the RIXS to the HAXPES, both spectroscopic techniques agree very well within experimental accuracy. This result suggests that the *total* RIXS intensity reflects the *total* sheet carrier density as does the Ti^{3+} contribution in HAXPES.

A caveat might be in order here. The electrons released by oxygen vacancies in STO are known to become trapped or itinerant with the ratio of the disproportionation depending on the positions of the oxygen vacancies with respect to the interface and/or their assembly to clusters [36–40]. As both RIXS components, dd excitations and fluorescence, increase in parallel upon doping [see Fig. 5(b)] one could be misled to assume that one signal originates from localized charge carriers (dd excitations) while the other feature reflects delocalized electrons (fluorescence) with a certain fixed disproportionation of the electrons between both. However, we have already ruled out this scenario for the reasons explained at the end of Sec. III B.

Finally, we show the sheet resistance of the three samples with different oxygen vacancy concentrations in Fig. 6(c). The data is in good agreement with those reported in a previous study on similar samples [41]. Since the charge carrier mobility at room temperature (RT) is essentially constant, the RT sheet resistance is a good measure for the *mobile* charge carrier concentration of samples with a confined 2DES. As can be seen from Fig. 6(c), the RT sheet resistance of the MP sample drops with respect to that of the PO sample pointing to a larger mobile charge carrier concentration in the former. The strong decrease of the RT sheet resistance for the LP sample, however, reflects for the main part not a strongly enhanced charge carrier concentration but the fact that here the conducting region is no longer confined to the interface and the charge transport hence three-dimensional [15]. Thus, the sheet resistance data is not suited to shed more light on the question of how to understand the physical nature of the two inelastic features in the RIXS spectra.

IV. DISCUSSION

The different behavior of the two components in RIXS of LAO/STO heterostructures upon varying the photon energy across the Ti L edge points to a different origin of these features. One signal stays at a constant energy loss and is identified as due to Raman processes, while the other feature shifts linearly with excitation energy and thus is ascribed to fluorescence decay. A previous assignment of these two features as originating from localized and itinerant Ti $3d$ charge carriers in the ground state is apparently inconsistent with our present data. Most strikingly, the observation of both RIXS components for the insulating 3-uc sample as well as their parallel rise in intensity upon increasing the film thickness before both features saturate at an overlayer thickness of 6 uc call for a different interpretation.

To form such an alternative view it is helpful to analyze the nature of the possible intermediate states in the RIXS experiment after the initial photoexcitation of a core electron into the Ti $3d$ shell in a simple TiO_6 cluster model, where the cluster may also be coupled to delocalized quantum states being a superposition of many different sites or conduction band states [42,43]. In the language of such a cluster model, two type of intermediate states may result that can account for the two types of features observed in our data. Firstly, the intermediate state can be of the type $2p^5 3d^1_{t_{2g}} 3d^1_{e_g}$ [see Fig. 7(a)]. In this case, both Ti $3d$ electrons stay localized at the same atomic site. By deexcitation of one $3d$ electron, the core hole created in the intial absorption is filled up again under emission of a photon. The energy difference between incoming and emitted photon reflects the associated electronic

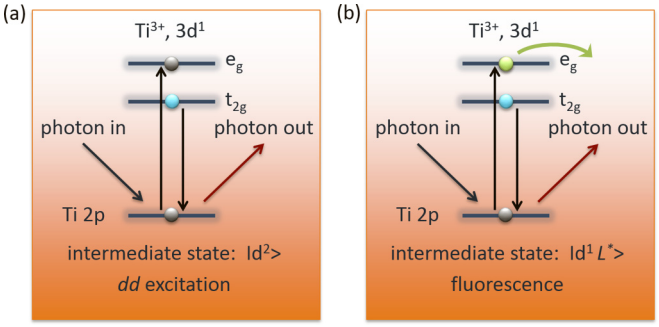

FIG. 7. Schematic drawing of two possible RIXS processes with different intermediate states. (a) The excited electron stays localized in the e_g states. After the decay process the final state is $3d^1_{e_g}$ (dd excitation, Raman signal). (b) The excited electron gets immediately delocalized which results in x-ray fluorescence. Here the final state is $3d^0$ (fluorescence signal). Our results can be explained by a superposition of these two different channels in the intermediate state.

dd excitation between the $3d$ t_{2g} and the e_g orbitals and appears in the RIXS spectra as a peak at finite energy loss with respect to the elastic line. The energy loss is independent of the incoming photon energy.

Secondly, assuming that one Ti $3d$ electron gets delocalized following the photoexcitation, the intermediate state is of the type $2p^5 3d^1_{t_{2g}} L^*$ with * denoting a delocalized state, involving many sites, or a conduction band state occupied with an extra electron [see Fig. 7(b)]. The probability for this intermediate state will be higher, if the TiO_6 cluster considered is more strongly coupled to its environment through hybridization. Here, a $3d$ valence electron decays radiatively into the $2p$ core hole generated by the preceding photoexcitation of an electron into delocalized states. After the radiative decay, the final state is of the type $2p^6 3d^0$ and corresponds to x-ray fluorescence. The energy of the fluorescence signal in such a transition is independent of the excitation energy and its intensity reflects essentially the occupied $3d^1_{t_{2g}}$ density of states.

Taking both decay channels into account, the intermediate state can be generally written as $\alpha|2p^5 3d^2> + \beta|2p^5 3d^1 L^*>$, where the relative weight of the Raman and fluorescence signal is given by $|\alpha|^2$ and $|\beta|^2$ (with $|\alpha|^2 + |\beta|^2 = 1$), respectively. Therefore the observation of either the Raman or the fluorescence signal reflects the electronic character of the intermediate states rather than the itinerancy or localized character of the Ti $3d$ electrons in the ground state.

The occurrence of Raman and fluorescence features like in our data has been previously reported for rutile TiO_2 [44,45] and, in the wake of it, theoretically analyzed by Ide and Kotani based on d-p cluster models [46,47]. If the cluster size is small, the excited electron stays localized. The inelastic peaks hence are caused by local excitations and shift linearly with incident photon energy. When the cluster size is enhanced, additional peaks appear that do not follow the change in incident photon energy. These originate from the occurrence of quantum states being a superposition of many different sites in the intermediate state of large clusters. The deexcitation of such states gives rise to the fluorescence peaks in the RIXS spectra [46,47]. Similar behavior has been observed in RIXS spectra on other compounds, e.g., on $BaTiO_3$ and $BaSO_4$ [31] or on $La_xSr_{1-x}TiO_3$ [26]. More complex behavior along these lines has been reported for charge-orbital-lattice coupling effects in one-dimensional cuprates [48] and spin versus charge excitations in superconducting cuprates [49,50] and related compounds [51].

V. SUMMARY

We have investigated LAO/STO heterostructures with varying LAO overlayer thickness and oxygen vacancy concentration by means of RIXS at the Ti L edge. Already for the sample with a 3-uc-thick film, i.e., below the critical thickness for conductivity, we have observed finite spectral weight, signaling that localized charge carriers are present in the ground state. This finding is in line with the report on ferromagnetism which has been ascribed to the local moments of trapped electrons. As seen previously on LAO/STO superlattices, we also have observed two types of contributions to the RIXS spectra due to dd excitations and fluorescence. They behave differently upon the variation of the excitation energy. A detailed analysis for samples with different film thicknesses and oxygen vacancy concentrations in combination with HAXPES results reveals the physical meaning of these two contributions at variance with previous interpretations. The appearance of fluorescence in addition to Raman features essentially reflects the finite probability for the excited electron to escape from the Ti ion in the coherent RIXS process, enabled by the complex, nonlocal nature of the intermediate state. Thus the Raman and fluorescence intensities are not simply related to the amounts of either the localized or itinerant charge carriers in the ground state. By comparing the total RIXS intensity (sum of dd excitations and fluorescence signal) and the Ti^{3+}/Ti^{4+} ratio obtained from HAXPES measurements, we conclude that the total RIXS intensity reflects the total amount of charge carriers (localized and delocalized) present in the system within experimental accuracy.

ACKNOWLEDGMENTS

Funding by the Deutsche Forschungsgemeinschaft (FOR 1162) is gratefully acknowledged. Experiments at SPring-8 BL07LSU were performed jointly by the Synchrotron Radiation Research Organization and the University of Tokyo (Proposal No. 2012A7429, No. 2012B7439, and No. 2013A7449). This work was financially supported by a Grants-in-Aid for Young Scientists (23740240) from the Ministry of Education, Culture, Sports, Science and Technology, Japan. We thank Y. Nishitani and Y. Nakata for supporting the experiments.

[1] A. Othomo and H. Y. Hwang, Nature (London) **427**, 423 (2004).

[2] S. Thiel, G. Hammerl, A. Schmehl, C. W. Schneider, and J. Mannhart, Science **313**, 1942 (2006).

[3] M. Sing, G. Berner, K. Goß, A. Müller, A. Ruff, A. Wetscherek, S. Thiel, J. Mannhart, S. A. Pauli, C. W. Schneider *et al.*, Phys. Rev. Lett. **102**, 176805 (2009).

[4] A. D. Caviglia, S. Gariglio, N. Reyren, D. Jaccard, T. Schneider, M. Gabay, S. Thiel, G. Hammerl, J. Mannhart, and J.-M. Triscone, Nature (London) **456**, 624 (2008).

[5] N. Reyren, S. Thiel, A. D. Caviglia, L. F. Kourkoutis, G. Hammerl, C. Richter, C. W. Schneider, T. Kopp, A.-S. Rüetschi, D. Jaccard *et al.*, Science **317**, 1196 (2007).

[6] L. Li, C. Richter, J. Mannhart, and R. C. Ashoori, Nat. Phys. **7**, 762 (2011).

[7] J. A. Bert, B. Kalisky, C. Bell, M. Kim, Y. Hikita, H. Y. Hwang, and K. A. Moler, Nat. Phys. **7**, 767 (2011).

[8] N. Pavlenko, T. Kopp, E. Y. Tsymbal, G. A. Sawatzky, and J. Mannhart, Phys. Rev. B. **85**, 020407 (R) (2012).

[9] C. Lin and A. A. Demkov, Phys. Rev. Lett. **113**, 157602 (2014).

[10] N. Nakagawa, H. Y. Hwang, and D. A. Muller, Nat. Mater. **5**, 204 (2006).

[11] L. Yu and A. Zunger, Nat. Commun. **5**, 5118 (2014).

[12] A. Kalabukhov, R. Gunnarsson, J. Börjesson, E. Olsson, T. Claeson, and D. Winkler, Phys. Rev. B **75** 121404(R) (2007).

[13] Z. Q. Liu, C. J. Li, W. M. Lü, X. H. Huang, Z. Huang, S. W. Zeng, X. P. Qiu, L. S. Huang, A. Annadi, J. S. Chen *et al.*, Phys. Rev. X **3** 021010 (2013).

[14] L. Dudy, M. Sing, P. Scheiderer, J. D. Denlinger, P. Schtz, J. Gabel, M. Buchwald, C. Schlueter, T.-L. Lee, and R. Claessen, Adv. Mater. **28**, 7443 (2016).

[15] C. Cancellieri, N. Reyren, S. Gariglio, A. D. Caviglia, A. Fête, and J.-M. Triscone, Europhys. Lett. **91**, 17004 (2010).

[16] M. Basletic, J.-L. Maurice, C. Carrétéro, G. Herranz, O. Copie, M. Bibes, E. Jacquet, K. Bouzehouane, S. Fusil, and A. Barthélémy, Nat. Mater. **7**, 621 (2008).

[17] G. Berner, M. Sing, H. Fujiwara, A. Yasui, Y. Saitoh, A. Yamasaki, Y. Nishitani, A. Sekiyama, N. Pavlenko, T. Kopp *et al.*, Phys. Rev. Lett. **110**, 247601 (2013).

[18] P. Schütz, F. Pfaff, P. Scheiderer, Y. Z. Chen, N. Pryds, M. Gorgoi, M. Sing, and R. Claessen, Phys. Rev. B. **91**, 165118 (2015).

[19] C. Cancellieri, A. S. Mishchenko, U. Aschauer, A. Filippetti, C. Faber, O. S. Barisic, V. A. Rogalev, T. Schmitt, N. Nagaosa, and V. N. Strocov, Nat. Commun. **7**, 10386 (2016).

[20] G. Berner, S. Glawion, J. Walde, F. Pfaff, H. Hollmark, L.-C. Duda, S. Paetel, C. Richter, J. Mannhart, M. Sing *et al.*, Phys. Rev. B. **82**, 241405(R) (2010).

[21] K.-J. Zhou, M. Radovic, J. Schlappa, V. Strocov, R. Frison, J. Mesot, L. Patthey, and T. Schmitt, Phys. Rev. B. **83**, 201402 (R) (2011).

[22] P. Scheiderer, F. Pfaff, J. Gabel, M. Kamp, M. Sing, and R. Claessen, Phys. Rev. B **92**, 195422 (2015).

[23] Y. Harada, M. Kobayashi, H. Niwa, Y. Senba, H. Ohashi, T. Tokushima, Y. Horikawa, S. Shin, and M. Oshima, Rev. Sci. Instrum. **83**, 013116 (2012).

[24] J. Gabel, M. Zapf, P. Scheiderer, P. Schütz, L. Dudy, M. Stübinger, C. Schlueter, T.-L. Lee, M. Sing, and R. Claessen, Phys. Rev. B **95**, 195109 (2017).

[25] C. Ulrich, G. Ghiringhelli, A. Piazzalunga, L. Braicovich, N. B. Brookes, H. Roth, T. Lorenz, and B. Keimer, Phys. Rev. B **77**, 113102 (2008).

[26] T. Higuchi, T. Tsukamoto, M. Watanabe, M. M. Grush, T. A. Callcott, R. C. Perera, D. L. Ederer, Y. Tokura, Y. Harada, and Y. Tezuka, Phys. Rev. B **60**, 7711 (1999).

[27] S. Tanuma, C. J. Powell, and D. R. Penn, Surf. Interface Anal. **21** 165 (1994).

[28] J. Strempfer, S. Francoual, D. Reuther, D. K. Shukla, A. Skaugen, H. Schulte-Schrepping, T. Kracht, and H. Franz, J. Synchrotron Radiat. **20**, 541 (2013).

[29] A. Fujimori and F. Minami, Phys. Rev. B **30**, 957 (1984).

[30] A. E. Bocquet, T. Mizokawa, K. Morikawa, A. Fujimori, S. R. Barman, K. Maiti, D. D. Sarma, Y. Tokura, and M. Onoda, Phys. Rev. B **53**, 1161 (1996).

[31] K. Yoshii, I. Jarrige, C. Suzuki, D. Matsumura, Y. Nishihata, Y. Yoneda, T. Fukuda, K. Tamura, Y. Ito, T. Mukoyama *et al.*, J. Phys. Chem. Solids **73**, 1106 (2012).

[32] M. Takizawa, S. Tsuda, T. Susaki, H. Y. Hwang, and A. Fujimori, Phys. Rev. B **84**, 245124 (2011).

[33] M. Salluzzo, S. Gariglio, X. Torrelles, Z. Ristic, R. D. Capua, J. Drnec, M. M. Sala, G. Ghiringhelli, R. Felici, and N. B. Brookes, Adv. Mater. **25**, 2333 (2013).

[34] B. Kalisky, J. A. Bert, B. B. Klopfer, C. Bell, H. K. Sato, M. Hosoda, Y. Hikita, H. Y. Hwang, and K. A. Moler, Nat. Commun. **3**, 922 (2012).

[35] M. Salluzzo, J. C. Cezar, N. B. Brookes, V. Bisogni, G. M. D. Luca, C. Richter, S. Thiel, J. Mannhart, M. Huijben, A. Brinkman *et al.*, Phys. Rev. Lett. **102**, 166804 (2009).

[36] D. D. Cuong, B. Lee, K. M. Choi, H.-S. Ahn, S. Han, and J. Lee, Phys. Rev. Lett. **98**, 115503 (2007).

[37] Z. Hou and K. Terakura, J. Phys. Soc. Jpn. **79**, 114704 (2010).

[38] N. Pavlenko, T. Kopp, E. Y. Tsymbal, J. Mannhart, and G. A. Sawatzky, Phys. Rev. B **86**, 064431 (2012).

[39] C. Lin and A. A. Demkov, Phys. Rev. Lett. **111**, 217601 (2013).

[40] H. O. Jeschke, J. Shen, and R. Valenti, New J. Phys. **17**, 023034 (2015).

[41] A. Brinkman, M. Huijben, M. van Zalk, J. Huijben, U. Zeitler, J. C. Maan, W. G. van der Wiel, G. Rijnders, D. H. A. Blank, and H. Hilgenkamp, Nat. Mater. **6**, 493 (2007).

[42] K. Horiba, M. Taguchi, A. Chainani, Y. Takata, E. Ikenaga, D. Miwa, Y. Nishino, K. Tamasaku, M. Awaji, A. Takeuchi *et al.*, Phys. Rev. Lett. **93**, 236401 (2004).

[43] Y. Ishida, R. Eguchi, M. Matsunami, K. Horiba, M. Taguchi, A. Chainani, Y. Senba, H. Ohashi, H. Ohta, and S. Shin, Phys. Rev. Lett. **100**, 056401 (2008).

[44] Y. Tezuka, S. Shin, A. Agui, M. Fujisawa, and T. Ishii, J. Phys. Soc. Jpn. **65**, 312 (1996).

[45] Y. Harada, T. Kinugasa, R. Eguchi, M. Matsubara, A. Kotani, M. Watanabe, A. Yagishita, and S. Shin, Phys. Rev. B **61**, 12854 (2000).

[46] T. Ide and A. Kotani, J. Phys. Soc. Jpn. **67**, 3621 (1998).

[47] T. Ide and A. Kotani, J. Phys. Soc. Jpn. **69**, 1895 (2000).

[48] J. J. Lee, B. Moritz, W. S. Lee, M. Yi, C. J. Jia, A. P. Sorini, K. Kudo, Y. Koike, K. J. Zhou, C. Monney *et al.*, Phys. Rev. B **89**, 041104 (2014).

[49] M. Guarise, B. Dalla Piazza, H. Berger, E. Giannini, T. Schmitt, H. M. Ronnow, G. A. Sawatzky, J. van den Brink, D. Altenfeld, I. Eremin *et al.*, Nat. Commun. **5**, 5760 (2014).

[50] H. Y. Huang, C. J. Jia, Z. Y. Chen, K. Wohlfeld, B. Moritz, T. P. Devereaux, W. B. Wu, J. Okamoto, W. S. Lee, M. Hashimoto *et al.*, Sci. Rep. **6**, 19657 (2016).

[51] M. Guarise, B. Dalla Piazza, M. Moretti Sala, G. Ghiringhelli, L. Braicovich, H. Berger, J. N. Hancock, D. van der Marel, T. Schmitt, V. N. Strocov *et al.*, Phys. Rev. Lett. **105**, 157006 (2010).